Staggered DG Methods on Polygonal Meshes

Eun-Jae Park

Computational Science & Engineering
School of Mathematics and Computing
Yonsei University, Seoul, Korea

UC-Irvine

ERC Workshop GATIPOR 2020+2
INRIA Paris
June 8-10, 2022

Outline

Motivation: Why polygonal meshes?

The interest for general meshes is recently growing:

- Easier/better meshing of domain (and data) features
- Automatic inclusion of "hanging nodes"
- Adaptivity: more efficient mesh refinement/coarsening
- Robustness to mesh distortion
- Topology optimization, Cracks, Fractures
- Interface, Multiphysics
- ......

Some literature

- Mimetic finite difference (MFD) method
- Multipoint flux approximation (MPFA) method
- Polygonal DG (Antonietti, Cangiani, Houston, . . .)
- Hybrid high order (HHO) method (Di Pietro, Ern, . . .)
- Virtual element method (VEM) (Beirão Da Veiga, Brezzi, Cangiani, Manzini, Marini, Russo, . . .)
- Weak Galerkin (WG) method (Wang, Ye, . . .)
- Staggered DG method (Zhao and Park, SISC'18)
- . . . . . .

Goal: New framework

To develop Staggered DG (SDG) methods of arbitrary polynomial orders on general polygonal meshes that offer the following features:

- Easier/better meshing of domain (and data) features
- Arbitrary shapes of polygon including small edges
- Robust to mesh distortion
- Automatic inclusion of hanging nodes
- No stabilization or penalty terms
- Local and global conservations
- Superconvergence and postprocessing
- Unfitted meshes are allowed

Polygonal SDG

- L. Zhao and E.-J. Park (SISC '18)
  - Inspired from triangular SDG method: Chung and Engquist (SINUM '06,'09)
  - **The lowest order polygonal SDG** for the Poisson equation
  - Reliable and efficient error estimators
- L. Zhao, E.-J. Park, and D.-w. Shin (CMAME '19)
  - The lowest order polygonal SDG for **the Stokes problem**
  - Guaranteed error estimators via equilibrated stress recon.
- Dohyun Kim, L. Zhao, and E.-J. Park (SISC '20)
  - **Arbitrary high order polygonal SDG** for the Stokes problem
- L. Zhao, E.-J. Park (SISC '20)
  - Staggered cell-centered DG for **linear elasticity**
- L. Zhao, E. Chung, E.-J. Park, and G. Zhou (SINUM '21)
  - **Darcy-Forchheimer** and Stokes coupling

Polygonal SDG

- L. Zhao, Dohyun Kim, E.-J. Park, and E. Chung (JSC '22)
  - Darcy flows in **fractured porous media**
- Sanghee Lee, Dohyun Kim, and E.-J. Park - Expanded SDG for anisotropic diffusion: a priori and a posteriori error analysis
- Dohyun Kim, L. Zhao, E. Chung, and E.-J. Park (arXiv'21)
  - **Pressure-robust** SDG for the **Navier-Stokes**
  - Exactly divergence free velocity
  - Arbitrary high order polygonal elements
- L. Zhao, E. Chung, and E.-J. Park (arXiv'20)
  - **Biot's system** of poroelasticity
  - **Arbitrary high order polygonal elasticity elements**

Outline

Poisson model: (Joint with Lina Zhao, SIAM J. Sci. Comput. 2018)

Consider the Poisson model problem:

$$
\begin{aligned}
-\Delta u = f \quad & \text{in } \Omega, \\
u = 0 \quad & \text{on } \partial\Omega.
\end{aligned}
$$

By introducing $\boldsymbol{p} = -\nabla u$, we obtain the first order system

$$
\begin{aligned}
\boldsymbol{p} &= -\nabla u, \\
\nabla \cdot \boldsymbol{p} &= f.
\end{aligned}
$$

- Inspired from standard SDG method on triangular meshes by Chung and Engquist (SINUM 2006,2009)

Staggered grids

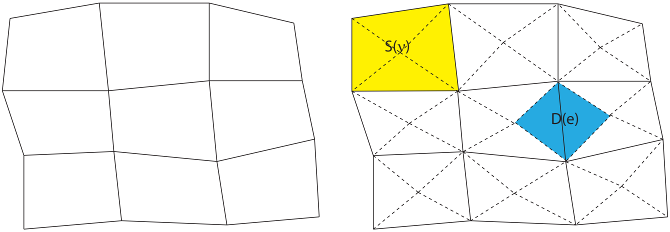

Figure: Initial mesh (left) and the resulting mesh (right).

$\mathcal{T}_u$ denotes the initial (primal) partition of the domain Ω,
$\mathcal{F}_u$ denotes primal edges, $\mathcal{F}_u^0$ denotes interior primal edges and $\mathcal{F}_p$ denotes dual edges. $\mathcal{T}_h$ denotes the resulting submeshes

Typical assumptions

1. Every element $S(\nu)$ in $\mathcal{T}_u$ is star-shaped with respect to a ball of radius $\geq \rho h_{S(\nu)}$.
2. For every element $S(\nu) \in \mathcal{T}_u$ and every edge $e \in \partial S(\nu)$, it satisfies $h_e \geq \rho h_{S(\nu)}$, where h_e denotes the length of edge e and $h_{S(\nu)}$ denotes the diameter of $S(\nu)$.

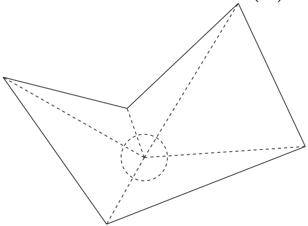

Figure: Shape regularity of a polygon.

Staggered finite element spaces

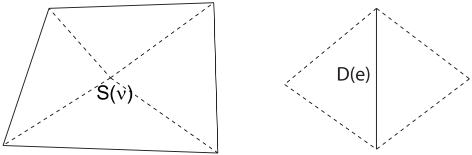

Figure: Schematic of primal mesh and dual mesh.

Finite element spaces on quadrilateral and polygonal meshes:

$$
\begin{aligned}
S_h :=& \{v : v\,|_\tau \in P_0(\tau),\ \forall \tau \in \mathcal{T}_h; [v]\,|_e = 0, e \in \mathcal{F}_u^0, v\,|_\tau = 0 \\
&\qquad\qquad\qquad\qquad \text{if } \partial\tau \cap \partial\Omega = e, e \in \mathcal{F}_u \backslash \mathcal{F}_u^0\}, \\
\boldsymbol{V}_h :=& \{\boldsymbol{q} : \boldsymbol{q}\,|_\tau \in P_0(\tau)^2, \forall \tau \in \mathcal{T}_h; [\boldsymbol{q}\cdot\boldsymbol{n}]\,|_e = 0, e \in \mathcal{F}_p\},
\end{aligned}
$$

where $\mathcal{F}_u$ denotes primal edges, $\mathcal{F}_u^0$ denotes interior primal edges and $\mathcal{F}_p$ denotes dual edges.

Degrees of freedom

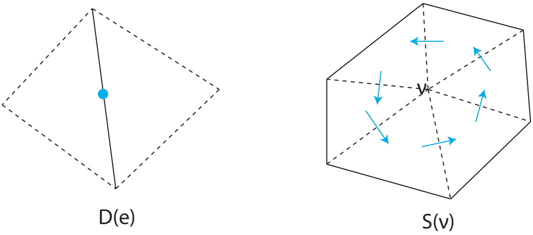

Figure: Degrees of freedom for S_h (left) and for $\boldsymbol{V}_h$ (right).

$v \in S_h$ is determined by the following degrees of freedom:

$$\phi_e(v) = \int_e v \, ds \quad \forall e \in \mathcal{F}_u.$$

$\boldsymbol{p} \in \boldsymbol{V}_h$ is determined by the following degrees of freedom:

$$\psi_e(\boldsymbol{p}) = \int_e \boldsymbol{p} \cdot \boldsymbol{n} \quad \forall e \in \mathcal{F}_p.$$

Other possible subdivision

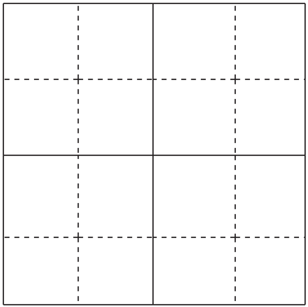

Figure: Subdivision into quadrilaterals.

Disadvantage: not robust to mesh distortion

SDG formulation

Introduce an auxiliary variable $\boldsymbol{p} = -\nabla u$, we get the first order system:

$$\begin{aligned} \boldsymbol{p} &= -\nabla u, \\ \nabla \cdot \boldsymbol{p} &= f. \end{aligned}$$

Multiplying by test function $\boldsymbol{q} \in \boldsymbol{V}_h$ and integration by parts over each $S(\nu)$ implies

$$(\boldsymbol{p}, \boldsymbol{q})_{S(\nu)} = (u, \nabla \cdot \boldsymbol{q})_{S(\nu)} - (u, \boldsymbol{q} \cdot \boldsymbol{n})_{\partial S(\nu)}.$$

Similarly, we obtain

$$(\boldsymbol{p} \cdot \boldsymbol{n}, v)_{\partial D(e)} - (\boldsymbol{p}, \nabla v)_{D(e)} = (f, v)_{D(e)}.$$

SDG formulation

Summing the above equations over all $S(\nu)$ and $D(e)$, we can get the discrete formulation: Find $(u_h, \boldsymbol{p}_h) \in S_h \times \boldsymbol{V}_h$ such that

$$(\boldsymbol{p}_h, \boldsymbol{q}) - b_h^*(u_h, \boldsymbol{q}) = 0 \qquad \forall\, \boldsymbol{q} \in \boldsymbol{V}_h, \tag{1}$$

$$b_h(\boldsymbol{p}_h, v) = (f, v) \quad \forall\, v \in S_h, \tag{2}$$

where

$$b_h^*(u_h, \boldsymbol{q}) = -\sum_{e \in \mathcal{F}_u^0} (u_h, [\boldsymbol{q} \cdot \boldsymbol{n}])_e,$$

$$b_h(\boldsymbol{p}_h, v) = \sum_{e \in \mathcal{F}_p} (\boldsymbol{p}_h \cdot \boldsymbol{n}, [v])_e.$$

Remark

(Mass conservation) Taking v in (2) to be identically one in $D(e)$, we have

$$-(\boldsymbol{p}_h \cdot \boldsymbol{n}_D, 1)_{\partial D(e)} = (f, 1)_{D(e)},$$

where $\boldsymbol{n}_D$ is the outward unit normal vector of $D(e)$.

Inf-sup condition

Discrete H^1 norm and $H(\text{div},\Omega)$ semi-norm:

$$\|v\|_Z^2 = \sum_{e\in\mathcal{F}_p} h_e^{-1}\|[v]\|_{0,e}^2,$$

$$\|\boldsymbol{q}\|_{Z'}^2 = \sum_{e\in\mathcal{F}_u^0} h_e^{-1}\|[\boldsymbol{q}\cdot\boldsymbol{n}]\|_{0,e}^2.$$

We have the inf-sup conditions:

$$\inf_{v\in S_h}\sup_{\boldsymbol{q}\in\boldsymbol{V}_h}\frac{b_h(\boldsymbol{q},v)}{\|v\|_Z\|\boldsymbol{q}\|_0}\geq\beta_1,$$

$$\inf_{\boldsymbol{q}\in\boldsymbol{V}_h}\sup_{v\in S_h}\frac{b_h^*(v,\boldsymbol{q})}{\|v\|_0\|\boldsymbol{q}\|_{Z'}}\geq\beta_2.$$

Error estimates

The L^2 error estimates with possibly low regularity can be stated in the next theorem.

Theorem

Assume that $(\boldsymbol{p}, u) \in (H^\epsilon(\Omega)^2 \cap H(\mathit{div}, \Omega)) \times H^{1+\epsilon}(\Omega), 0 < \epsilon \leq 1$. *Let* $(\boldsymbol{p}_h, u_h)$ *be the numerical solution, then there exists a positive constant* C *such that*

$$\|u - u_h\|_0 \leq C(h^{\min\{1,2\epsilon\}}\|u\|_{1+\epsilon} + (\sum_{\tau \in \mathcal{T}_h} h_\tau^2 \|f\|_{0,\tau}^2)^{1/2}),$$

$$\|\boldsymbol{p} - \boldsymbol{p}_h\|_0 \leq Ch^\epsilon \|u\|_{1+\epsilon}.$$

Postprocessing

Let $S_h^* = \{v\,|_\tau \in P_1(\tau)\ \forall \tau \in \mathcal{T}_h; v\,|_{\partial\Omega} = 0\}$, then we can define the postprocessing $u_h^* \in S_h^*$

$$\begin{aligned}(\nabla u_h^*, \nabla v_h)_\tau &= (\boldsymbol{p}_h, \nabla v_h)_\tau \quad \forall v_h \in P_1(\tau)/P_0(\tau),\\ \frac{(u_h^*, 1)_e}{|e|} &= u_h\,|_e \quad\ \forall e \in \mathcal{F}_u \cap \partial\tau.\end{aligned}$$

A posteriori error estimator

Let the local error estimator be defined as

$$\eta_\tau^2 = \sum_{e \in \mathcal{F} \cap \partial\tau} h_e \| [\boldsymbol{p}_h \cdot \boldsymbol{t}] \|_{0,e}^2 + \sum_{e \in \mathcal{F}_u^0 \cap \partial\tau} h_e \| [\boldsymbol{p}_h \cdot \boldsymbol{n}] \|_{0,e}^2 + h_\tau^2 \| f \|_{0,\tau}^2.$$

Then, the global error estimator can be defined by

$$\eta^2 = \sum_{\tau \in \mathcal{T}_h} \eta_\tau^2.$$

Theorem

Let $(\boldsymbol{p}, u)$ be the weak solution and $(\boldsymbol{p}_h, u_h)$ be the numerical solution, then there exists a positive constant C_{rel} such that

$$\|\boldsymbol{p} - \boldsymbol{p}_h\|_0 \leq C_{rel}\eta.$$

Local efficiency

Theorem

Let f_h be a piecewise constant approximation of f. Let $(\boldsymbol{p}, u)$ be the solution of the weak problem and $(\boldsymbol{p}_h, u_h)$ be the numerical solution. Then there exists a positive constant C independent of the meshsize such that

$$\eta_\tau \leq C(\|\boldsymbol{p} - \boldsymbol{p}_h\|_{0,D(e)} + (\sum_{\tau \in D(e)} h_\tau^2 \|f - f_h\|_{0,\tau}^2)^{1/2}).$$

Smooth solution on general meshes

$\Omega = (0,1)^2$ and the exact solution is given by

$$u = x(1-x)y(1-y).$$

Trapezoidal grid:

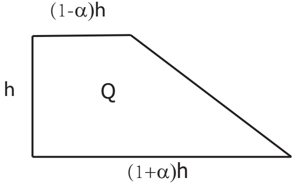

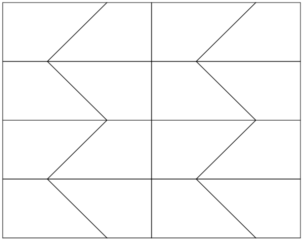

Figure: Partition of Ω.

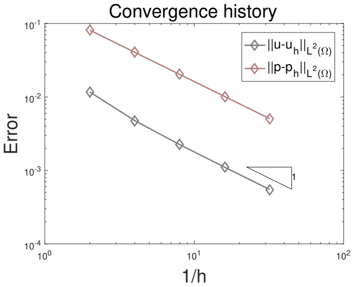

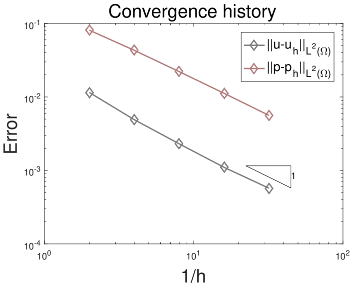

Figure: Convergence history for $\alpha = 0$ (left) and $\alpha = 0.4$ (right).

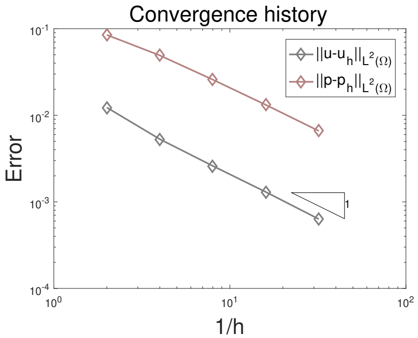

Figure: Convergence history for $\alpha = 0.8$.

Perturbed grid

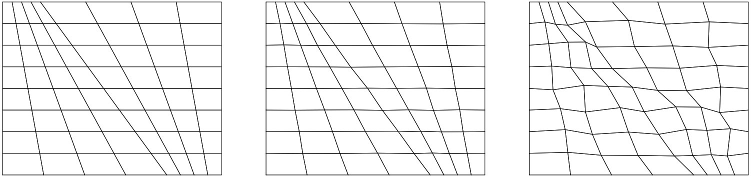

Figure: Grids used for simulations. From left to right: (a): Smooth grid. (b): Random h^2-perturbation of the smooth grid. (c): Random h-perturbation of the smooth grid.

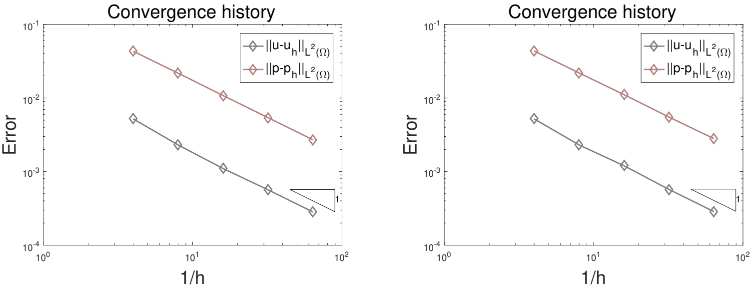

Figure: Convergence history for h^2-perturbation (left) and h-perturbation (right).

Polygonal mesh

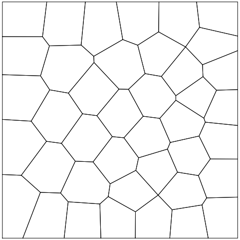

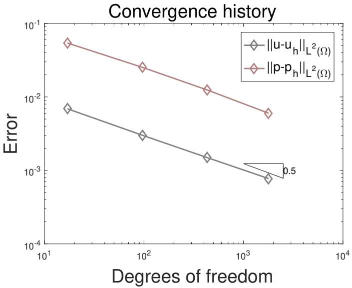

Figure: Partition of Ω into polygons (left) and convergence history (right).

Singular solution on L shaped domain

$u = r^{\frac{2}{3}} \sin(\frac{2\theta}{3})$

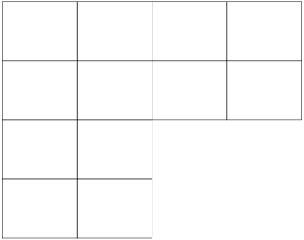

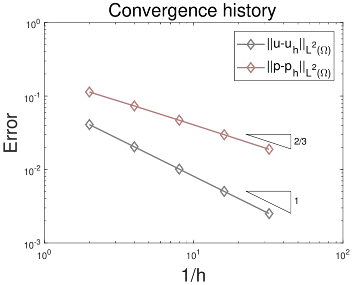

Figure: Initial mesh (left) and convergence history on uniform refinement (right).

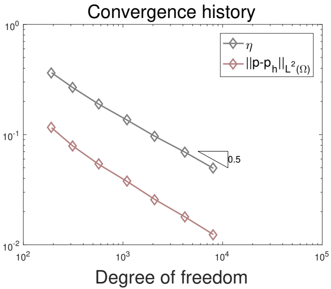

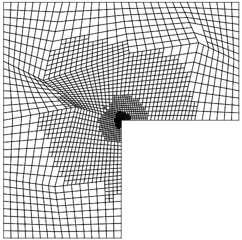

Figure: Convergence history for adaptive refinement (left) and adaptive mesh pattern (right).

Strong internal layer on unit square domain

$\Omega = (0,1)^2$ and the exact solution is given by

$$u = 16x(1-x)y(1-y)\arctan(25x - 100y + 50)$$

Although u is smooth, it has a strong internal layer along the line $y = 1/2 + x/4$.

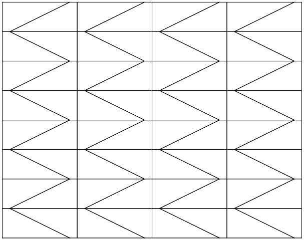

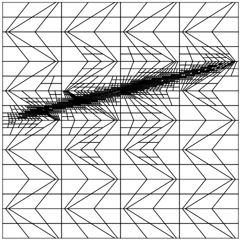

Figure: Initial mesh (left) and adaptive mesh (right).

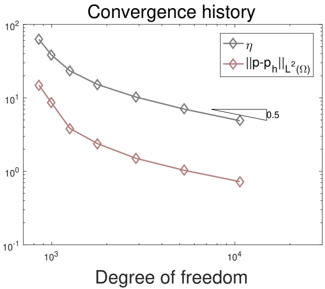

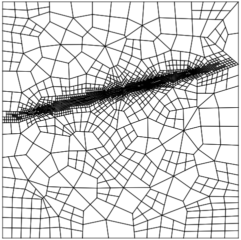

Figure: Convergence history for adaptive refinement (left) and adaptive mesh pattern (right).

Outline

Fracture Model: (Joint with L. Zhao, D. Kim, and E. Chung, JSC 2022)

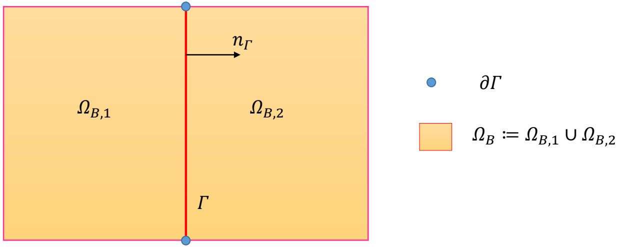

Figure: Illustration of bulk and fracture domain.

Fracture Model

In the bulk domain:

$$\begin{aligned} \boldsymbol{u} + K\nabla p &= \boldsymbol{0} \quad \text{in } \Omega_B, \\ \nabla \cdot \boldsymbol{u} &= f \quad \text{in } \Omega_B, \\ p &= p_0 \quad \text{on } \partial\Omega_B. \end{aligned} \tag{3}$$

On the fracture [1]:

$$\begin{aligned} -\nabla_t \cdot (K_\Gamma \nabla_t p_\Gamma) &= \ell_\Gamma f_\Gamma + [\boldsymbol{u} \cdot \boldsymbol{n}_\Gamma] && \text{in } \Gamma, \\ p_\Gamma &= g_\Gamma && \text{on } \partial\Gamma. \end{aligned} \tag{4}$$

The jump condition:

$$\begin{aligned} \eta_\Gamma \{\boldsymbol{u} \cdot \boldsymbol{n}_\Gamma\} &= [p] && \text{on } \Gamma, \\ \alpha_\Gamma [\boldsymbol{u} \cdot \boldsymbol{n}_\Gamma] &= \{p\} - p_\Gamma && \text{on } \Gamma. \end{aligned} \tag{5}$$

[1] V. Martin, J. Jaffré, and J. E. Roberts, Modeling fractures and barriers as interfaces for flow in porous media, SISC '05

Polygonal Mesh

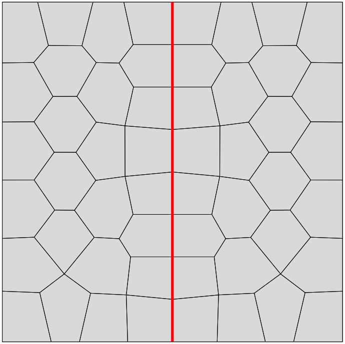

Figure: A fitted polygonal mesh to the fractured porous media.

Polygonal Mesh - Subdivision

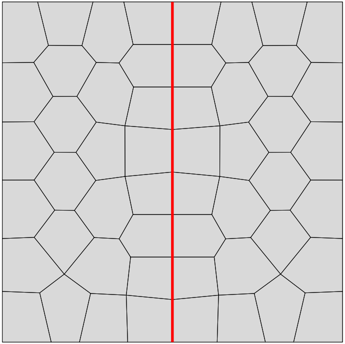

Figure: Schematic of staggered mesh. $S(\nu)$ is a primal element and $D(e)$ is a dual element. Here, —— are primal edges $\mathcal{F}_{pr}$ and - - - are dual edges $\mathcal{F}_{dl}$.

Polygonal Mesh - Subdivision

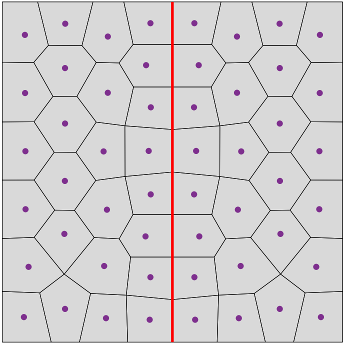

Figure: Schematic of staggered mesh. $S(\nu)$ is a primal element and $D(e)$ is a dual element. Here, —— are primal edges $\mathcal{F}_{pr}$ and - - - are dual edges $\mathcal{F}_{dl}$.

Polygonal Mesh - Subdivision

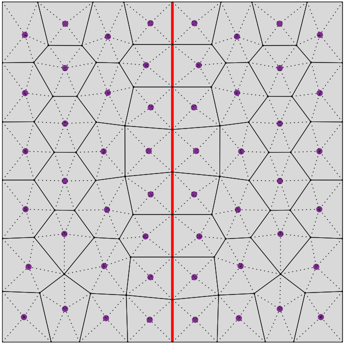

Figure: Schematic of staggered mesh. $S(\nu)$ is a primal element and $D(e)$ is a dual element. Here, —— are primal edges $\mathcal{F}_{pr}$ and - - - are dual edges $\mathcal{F}_{dl}$.

Polygonal Mesh - Subdivision

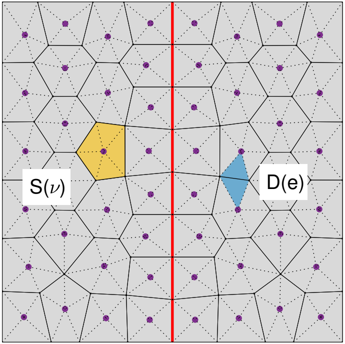

Figure: Schematic of staggered mesh. $S(\nu)$ is a primal element and $D(e)$ is a dual element. Here, —— are primal edges $\mathcal{F}_{pr}$ and - - - are dual edges $\mathcal{F}_{dl}$.

Discrete space

We introduce three spaces

$$\begin{aligned} \boldsymbol{u}_h \in V_h &= [\mathbb{P}_k(\mathcal{T}_h)]^2 \cap H(\mathrm{div}; \mathcal{S}(\mathcal{N})), \\ p_h \in S_h &= \mathbb{P}_k(\mathcal{T}_h) \cap H^1(\mathcal{D}(\mathcal{F}_{dl})), \\ p_{\Gamma,h} \in W_h &= \mathbb{P}_k(\mathcal{F}_h^\Gamma) \cap H_0^1(\Gamma). \end{aligned}$$

Discrete space - Velocity

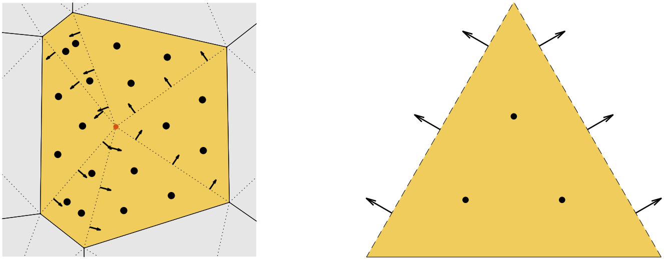

Figure: DOFs of quadratic velocity variable on a primal element.

$$
\begin{aligned}
V_h &= \{\boldsymbol{\psi} \in [\mathbb{P}_k(\mathcal{T}_h)]^2 : \boldsymbol{\psi}|_{S(\nu)} \in H(\mathsf{div}; S(\nu)) \ \forall \nu \in \mathcal{N}\} \\
&= \{\boldsymbol{\psi} \in [\mathbb{P}_k(\mathcal{T}_h)]^2 : [\![\boldsymbol{\psi} \cdot \mathbf{n}]\!] = 0 \ \forall e \in \mathcal{F}_{dl}\}
\end{aligned}
$$

Discrete space - Pressure

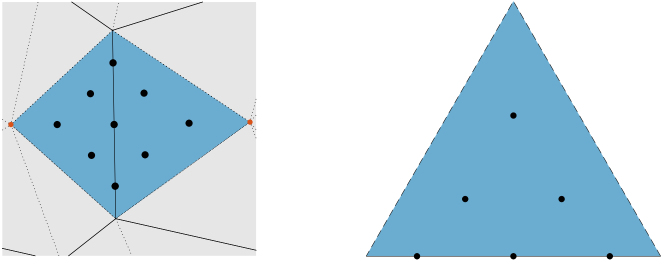

Figure: DOFs of quadratic pressure variable on a dual element.

$$S_h = \{v \in \mathbb{P}_k(\mathcal{T}_h) : v|_{\mathcal{D}(e)} \in C^0(\mathcal{D}(e)) \; \forall e \in \mathcal{F}_{pr}\}$$
$$= \{v \in \mathbb{P}_k(\mathcal{T}_h) : [\![v]\!] = 0 \; \forall e \in \mathcal{F}_{pr}\}$$

Discrete Space - Fracture

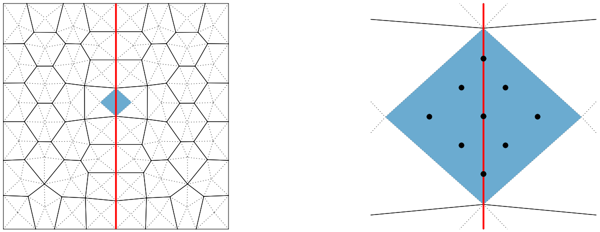

Figure: DOFs of quadratic pressure variable on a dual element with $e \subset \Gamma$.

Discrete Space - Fracture

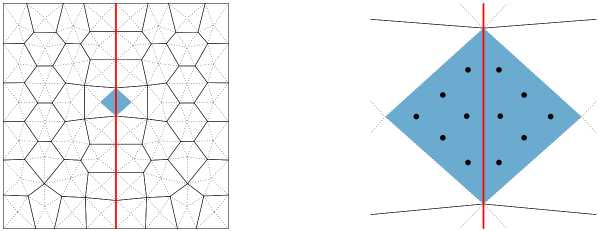

Figure: DOFs of quadratic pressure variable on a dual element with $e \subset \Gamma$.

Discrete Space - Fracture

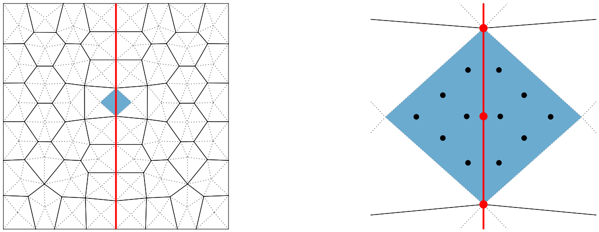

Figure: DOFs of quadratic pressure variable on a dual element with $e \subset \Gamma$.

$$W_h = \{q_\Gamma \in H_0^1(\Gamma) : q_\Gamma|_e \in \mathbb{P}_k(\mathcal{F}_h^\Gamma)\}.$$

Discrete Spaces - Norms

The discrete spaces are equipped with norms

$$\|q\|_{1,h}^2 = \|\nabla q\|_{L^2(\mathcal{T}_h)}^2 + \sum_{\tau \in \mathcal{T}_h} \sum_{e \in \mathcal{F}_{dl} \cap \partial\tau} \frac{h_e}{2|\tau|} \|[\![q]\!]\|_{L^2(e)}^2$$

$$\|\boldsymbol{v}\|_{0,h}^2 = \|\boldsymbol{v}\|_{L^2(\mathcal{T}_h)}^2 + \sum_{\tau \in \mathcal{T}_h} \sum_{e \in \mathcal{F}_{pr} \cap \partial\tau} \frac{2|\tau|}{h_e} \|[\![\boldsymbol{v} \cdot \mathbf{n}]\!]\|_{L^2(e)}^2$$

$$\|q_\Gamma\|_{1,\Gamma}^2 = \|\nabla q_\Gamma\|_{L^2(\Gamma)}^2 .$$

Assumptions on Mesh

We consider the following assumptions on the polygonal mesh:

Assumption (A) Every $S(\nu) \in \mathcal{T}_u$ is **star-shaped with respect to a ball** of radius $\geq \rho_S h_{S(\nu)}$.
$\Rightarrow$ Guarantees **valid** triangulation $\mathcal{T}_h$.

Assumption (B) For each $S(\nu) \in \mathcal{T}_u$ and $e \in \partial S(\nu)$, it satisfies $h_e \geq \rho_E h_{S(\nu)}$.
$\Rightarrow$ Guarantees **shape-regular** triangulation $\mathcal{T}_h$.

SDG Interpolation

We introduce the SDG interpolations by

$$\begin{aligned}
\langle I_h q - q, \psi\rangle_e = 0 &\quad \forall \psi \in \mathbb{P}_k(e),\ e \in \mathcal{F}_{pr}\backslash\mathcal{F}_h^{\Gamma},\\
\langle (I_h q - q)|_{\Omega_{B,i}}, \psi\rangle_e = 0 &\quad \forall \psi \in \mathbb{P}_k(e),\ e \in \mathcal{F}_h^{\Gamma},\ i = 1, 2,\\
(I_h q - q, \psi)_\tau = 0 &\quad \forall \psi \in \mathbb{P}_{k-1}(\tau),\ \tau \in \mathcal{T}_h
\end{aligned}$$

and

$$\begin{aligned}
\langle (J_h \boldsymbol{v} - \boldsymbol{v}) \cdot \boldsymbol{n}, \phi\rangle_e = 0 &\quad \forall \phi \in \mathbb{P}_k(e),\ e \in \mathcal{F}_{dl},\\
(J_h \boldsymbol{v} - \boldsymbol{v}, \boldsymbol{\phi})_\tau = 0 &\quad \forall \boldsymbol{\phi} \in \mathbb{P}_{k-1}(\tau)^2,\ \tau \in \mathcal{T}_h.
\end{aligned}$$

Discrete Formulation

Find $(\boldsymbol{u}_h, p_h, p_{\Gamma,h})$ satisfying for all $(\boldsymbol{v}, q, q_\Gamma) \in \boldsymbol{V}_h \times S_h \times W_h$

$$\begin{aligned} (K^{-1}\boldsymbol{u}_h, \boldsymbol{v})_{\Omega_B} + b_h^*(p_h, \boldsymbol{v}) &= 0, \\ -b_h(\boldsymbol{u}_h, q) + J_h(p_h, q) + c_h((p_h, p_{\Gamma,h}), (q, 0)) &= (f, q)_{\Omega_B}, \\ \langle K_\Gamma \nabla_t p_{\Gamma,h}, \nabla_t q_\Gamma \rangle_\Gamma + c_h((p_h, p_{\Gamma,h}), (0, q_\Gamma)) &= \langle \ell_\Gamma f_\Gamma, q_\Gamma \rangle_\Gamma. \end{aligned} \tag{6}$$

Here,

$$\begin{aligned} b_h(\boldsymbol{u}_h, q) &= -\sum_{e \in \mathcal{F}_{dl}} \langle \boldsymbol{u}_h \cdot \boldsymbol{n}, [q] \rangle_e + \sum_{\tau \in \mathcal{T}_h} (\boldsymbol{u}_h, \nabla q)_\tau, \\ b_h^*(p_h, \boldsymbol{v}) &= \sum_{e \in \mathcal{F}_{pr}^0} \langle p_h, [\boldsymbol{v} \cdot \boldsymbol{n}] \rangle_e - \sum_{\tau \in \mathcal{T}_h} (p_h, \nabla \cdot \boldsymbol{v})_\tau \\ &\quad + \sum_{e \in \mathcal{F}_h^\Gamma} \langle [p_h(\boldsymbol{v} \cdot \boldsymbol{n})], 1 \rangle_e. \end{aligned}$$

Discrete Formulation

Find $(\boldsymbol{u}_h, p_h, p_{\Gamma,h})$ satisfying for all $(\boldsymbol{v}, q, q_\Gamma) \in \boldsymbol{V}_h \times S_h \times W_h$

$$\begin{aligned}
(K^{-1}\boldsymbol{u}_h, \boldsymbol{v})_{\Omega_B} + b_h^*(p_h, \boldsymbol{v}) &= 0, \\
-b_h(\boldsymbol{u}_h, q) + J_h(p_h, q) + c_h((p_h, p_{\Gamma,h}), (q, 0)) &= (f, q)_{\Omega_B}, \\
\langle K_\Gamma \nabla_t p_{\Gamma,h}, \nabla_t q_\Gamma \rangle_\Gamma + c_h((p_h, p_{\Gamma,h}), (0, q_\Gamma)) &= \langle \ell_\Gamma f_\Gamma, q_\Gamma \rangle_\Gamma.
\end{aligned} \tag{7}$$

Here,

$$J_h(p_h, q) = \sum_{e \in \mathcal{F}_h^\Gamma} \langle \frac{1}{\eta_\Gamma}[p_h], [q] \rangle_e$$

$$c_h((p_h, p_{\Gamma,h}), (q, q_\Gamma)) = \sum_{e \in \mathcal{F}_h^\Gamma} \langle \frac{1}{\alpha_\Gamma}(\{p_h\} - p_{\Gamma,h}), \{q\} - q_\Gamma \rangle_e.$$

Remark on Discrete Operators

- Discrete adjoint property:

$$b_h(\boldsymbol{v}, q) = b_h^*(q, \boldsymbol{v}) \quad \forall \boldsymbol{v}, q \in V_h \times S_h.$$

- For given $\boldsymbol{v} \in [H^1(\Omega)]^2$,

$$b_h(\boldsymbol{v} - J_h \boldsymbol{v}, q) = 0 \quad \forall q \in S_h$$

  and for given $q \in H_0^1(\Omega)$

$$b_h^*(q - I_h q, \boldsymbol{v}) = 0 \quad \forall \boldsymbol{v} \in V_h.$$

- Non-negativity:

$$J_h(q, q) = \sum_{e \in \mathcal{F}_h^\Gamma} \eta_\Gamma^{-1} \|[q]\|_{0,e}^2,$$

$$c_h((q, q_\Gamma), (q, q_\Gamma)) = \sum_{e \in \mathcal{F}_h^\Gamma} \alpha_\Gamma^{-1} \|\{q\} - q_\Gamma\|_{0,e}^2.$$

Discrete inf-sup

Lemma (Discrete inf-sup)

$$\inf_{q \in S_h} \sup_{\boldsymbol{v} \in \boldsymbol{V}_h} \frac{b_h(\boldsymbol{v}, q)}{\|\boldsymbol{v}\|_{0,h} \|q\|_{1,h}} \geq C.$$

Stability

Theorem (Stability)

The discrete system (7) *admits a unique solution* $(\boldsymbol{u}_h, p_h, p_{\Gamma,h}) \in \boldsymbol{V}_h \times S_h \times W_h$. *Furthermore, there exists a positive constant* C *such that*

$$\begin{aligned}
&\|K^{-\frac{1}{2}}\boldsymbol{u}_h\|^2_{0,\Omega_B} + K_{\min}\|p_h\|^2_{0,\Omega_B} \\
&\quad + \sum_{e\in\mathcal{F}_h^\Gamma} \|\eta_\Gamma^{-\frac{1}{2}}[p_h]\|^2_{0,e} + \|K_\Gamma^{\frac{1}{2}}\nabla_t p_{\Gamma,h}\|^2_{0,\Gamma} \\
&\quad + \sum_{e\in\mathcal{F}_h^\Gamma} \|\alpha_\Gamma^{-\frac{1}{2}}(\{p_h\} - p_{\Gamma,h})\|^2_{0,e} \\
&\le C\Big(K_{\min}^{-1}\|f\|^2_{0,\Omega_B} + K_{\Gamma,\min}^{-1}\|\ell_\Gamma f_\Gamma\|^2_{0,\Gamma}\Big).
\end{aligned} \tag{8}$$

Convergence

Theorem (Convergence)

There exists a positive constant C such that

$$
\begin{aligned}
&\|K^{-\frac{1}{2}}(J_h\boldsymbol{u}-\boldsymbol{u}_h)\|_{0,\Omega_B}+\|K_\Gamma^{\frac{1}{2}}\nabla_t(\Pi_h^p p_\Gamma-p_{\Gamma,h})\|_{0,\Gamma}\\
&+\Big(\sum_{e\in\mathcal{F}_h^\Gamma}\|\eta_\Gamma^{-\frac{1}{2}}[I_hp-p_h]\|_{0,e}^2\Big)^{\frac{1}{2}}\\
&\quad+\Big(\sum_{e\in\mathcal{F}_h^\Gamma}\|\alpha_\Gamma^{-\frac{1}{2}}(\{I_hp-p_h\}-(\Pi_h^p p_\Gamma-p_{\Gamma,h}))\|_{0,e}^2\Big)^{\frac{1}{2}}\\
&\le C\Big(\|K^{-\frac{1}{2}}(\boldsymbol{u}-J_h\boldsymbol{u})\|_{0,\Omega_B}+\|\alpha_\Gamma^{-\frac{1}{2}}(p_\Gamma-\Pi_h^p p_\Gamma)\|_{0,\Gamma}\Big)
\end{aligned}
$$

where the Ritz projection $\Pi_h^p : H_0^1(\Gamma)\to W_h$ is defined by

$$
\langle K_\Gamma\nabla_t\Pi_h^p p_\Gamma,\nabla_t q_{\Gamma,h}\rangle_\Gamma=\langle K_\Gamma\nabla_t p_\Gamma,\nabla_t q_{\Gamma,h}\rangle_\Gamma\quad\forall q_{\Gamma,h}\in W_h.
$$

Corollary

Assume that $(\boldsymbol{u}|_\tau, p|_\tau, p_\Gamma|_e) \in H^{k+1}(\tau)^2 \times H^{k+1}(\tau) \times H^{k+1}(e)$ *for* $\tau \in \mathcal{T}_h$ *and* $e \in \mathcal{F}_h^\Gamma$*. Then there exists a positive constant* C *such that*

$$\begin{aligned}
\|K^{-\frac{1}{2}}(\boldsymbol{u} - \boldsymbol{u}_h)\|_{0,\Omega_B} &\leq Ch^{k+1}, \\
\|p_\Gamma - p_{\Gamma,h}\|_{0,\Gamma} &\leq Ch^{k+1}, \\
\|p - p_h\|_{0,\Omega_B} &\leq Ch^{k+1}.
\end{aligned}$$

Example - 1

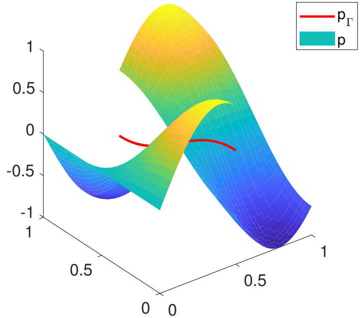

Figure: Graphs of solutions p and p_Γ for Example 1.

$$p = \begin{cases} \sin(4x)\cos(\pi y) & \text{in } \Omega_{B,1}, \\ \cos(4x)\cos(\pi y) & \text{in } \Omega_{B,2}, \end{cases} \qquad p_\Gamma = \frac{3}{4}\cos(\pi y)(\cos(2)+\sin(2)),$$

Permeable/Impermeable

We consider two different configuration for the physical constants.

$$\kappa_\Gamma^n = \begin{cases} 0.01 & \text{for impermeable case,} \\ 1 & \text{for permeable case.} \end{cases}$$

Other physical parameters are chosen as $\xi = 3/4$, $\ell_\Gamma = 0.01$, $K_\Gamma = 1$ and

$$K = \begin{pmatrix} \kappa_\Gamma^n/(2\ell_\Gamma) & 0 \\ 0 & 1 \end{pmatrix}.$$

Mesh configuration

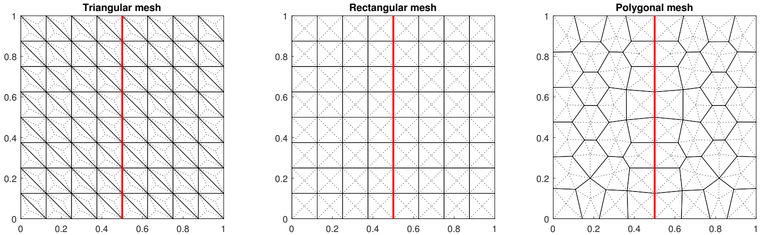

Figure: Uniform triangular (left), rectangular (center), polygonal (right) meshes with comparable mesh sizes for Example 1. Here, dashed lines represent dual edges and red lines are the fracture Γ.

Convergence History - Impermeable

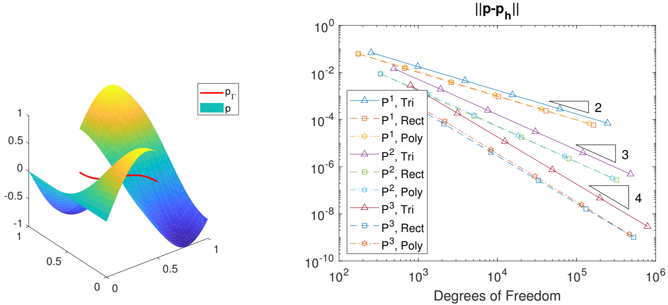

Figure: Convergence history for the impermeable case ($K_\Gamma = 0.01$) of Example 1 with $k = 1, 2, 3$. Right triangles indicate theoretical convergence rates. Solid lines, dotted lines, and dashed lines are error with triangular, rectangular, and polygonal meshes, respectively.

Convergence History - Impermeable

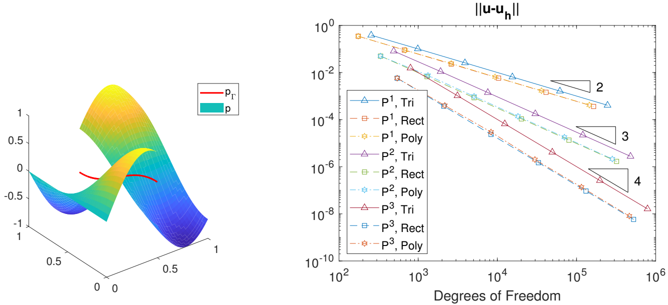

Figure: Convergence history for the impermeable case ($K_\Gamma = 0.01$) of Example 1 with $k = 1, 2, 3$. Right triangles indicate theoretical convergence rates. Solid lines, dotted lines, and dashed lines are error with triangular, rectangular, and polygonal meshes, respectively.

Convergence History - Impermeable

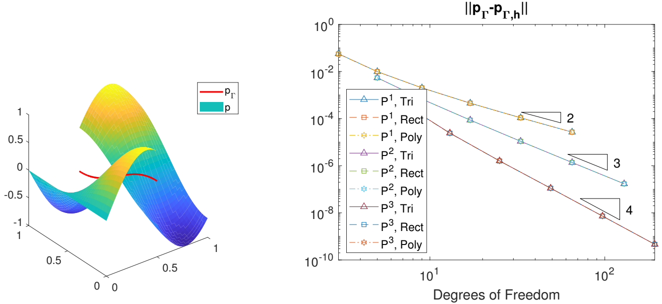

Figure: Convergence history for the impermeable case ($K_\Gamma = 0.01$) of Example 1 with $k = 1, 2, 3$. Right triangles indicate theoretical convergence rates. Solid lines, dotted lines, and dashed lines are error with triangular, rectangular, and polygonal meshes, respectively.

Convergence History - Permeable

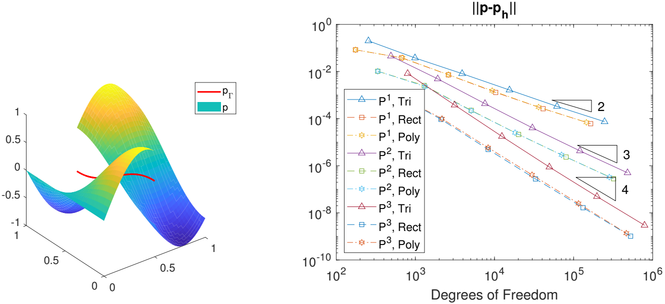

Figure: Convergence history for the permeable case ($K_\Gamma = 1$) of Example 1 with $k = 1, 2, 3$. Right triangles indicate theoretical convergence rates. Solid lines, dotted lines, and dashed lines are error with triangular, rectangular, and polygonal meshes, respectively.

Convergence History - Permeable

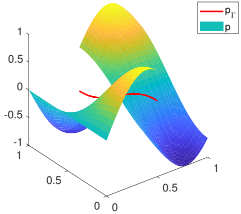

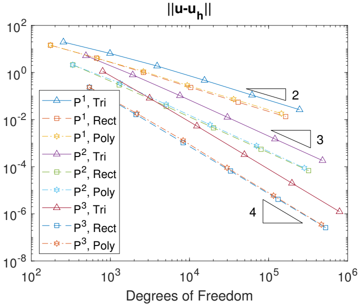

Figure: Convergence history for the permeable case ($K_\Gamma = 1$) of Example 1 with $k = 1, 2, 3$. Right triangles indicate theoretical convergence rates. Solid lines, dotted lines, and dashed lines are error with triangular, rectangular, and polygonal meshes, respectively.

Convergence History - Permeable

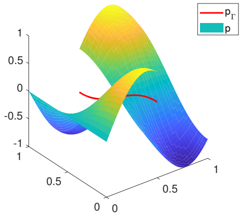

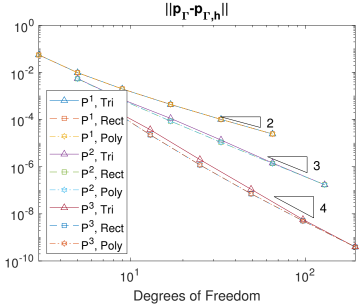

Figure: Convergence history for the permeable case ($K_\Gamma = 1$) of Example 1 with $k = 1, 2, 3$. Right triangles indicate theoretical convergence rates. Solid lines, dotted lines, and dashed lines are error with triangular, rectangular, and polygonal meshes, respectively.

Small Edge - Mesh Configuration

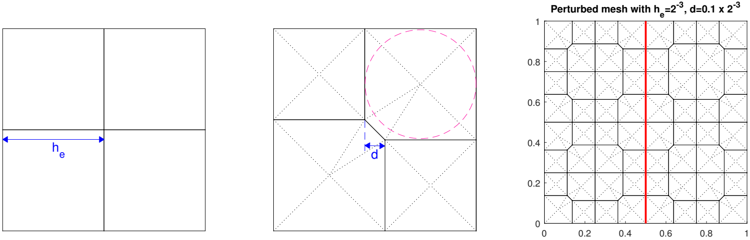

Figure: Schematic of perturbation. 2×2 squares (left), two rectangles and two pentagons after perturbation with $d = 0.1 \times h_e$ (center), and a resulting mesh from a uniform rectangular mesh with $h_e = 2^{-3}$ and $d = 0.1 \times h_e$. The dashed circle is the ball, described in Assumption (A), of an pentagon.

In the following example, we used $d = 0.001 \times h_e$.

Small Edge vs Rectangle

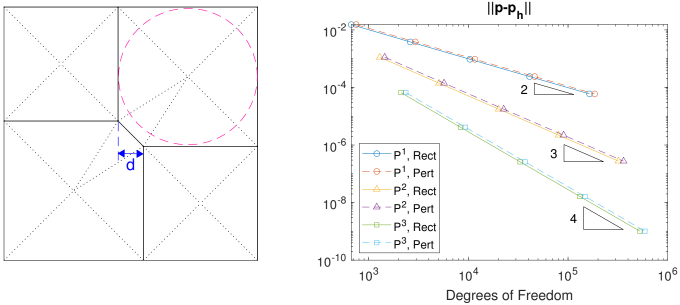

Figure: Convergence history with uniform rectangular meshes (solid lines) and perturbed meshes with $d = 0.001 \times h_e$ (dashed lines)

Small Edge vs Rectangle

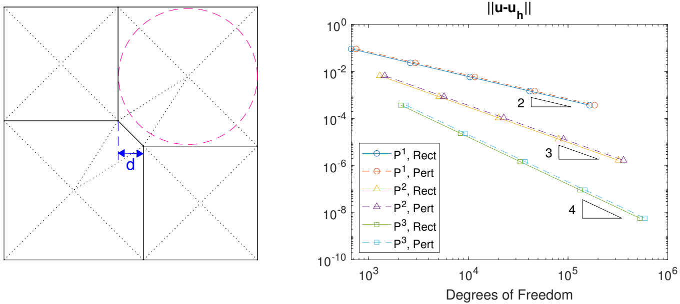

Figure: Convergence history with uniform rectangular meshes (solid lines) and perturbed meshes with $d = 0.001 \times h_e$ (dashed lines)

Small Edge vs Rectangle

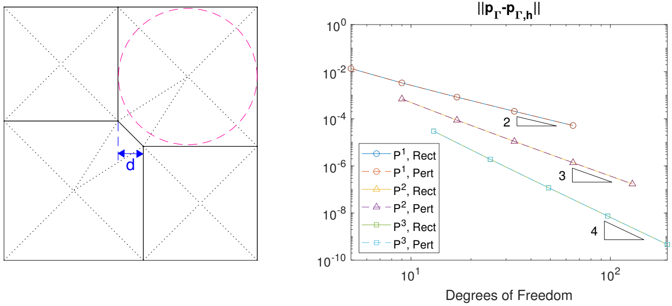

Figure: Convergence history with uniform rectangular meshes (solid lines) and perturbed meshes with $d = 0.001 \times h_e$ (dashed lines)

Unfitted Mesh

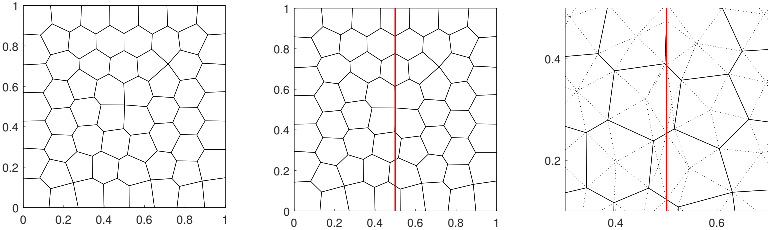

Figure: Underlying polygonal mesh ($\mathcal{T}_{pr}$, left), modified mesh ($\tilde{\mathcal{T}}_u$) (center) and its magnified view with dual edges (right). The modified mesh contains both sliver elements and small edges.

Unfitted Mesh - Convergence

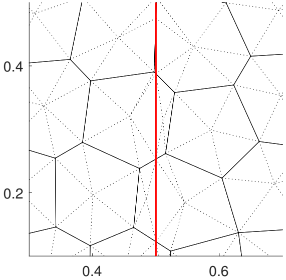

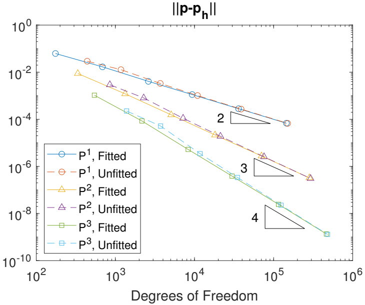

Figure: Convergence history with fitted (solid lines) and unfitted (dashed lines).

Unfitted Mesh - Convergence

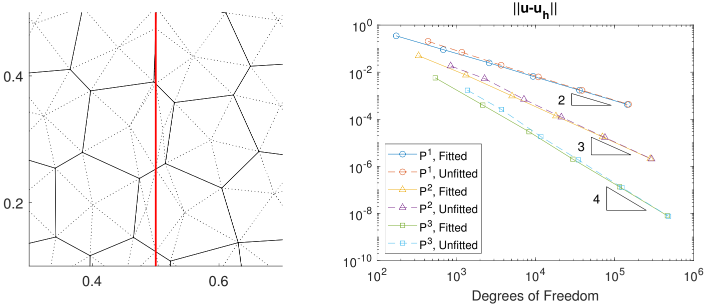

Figure: Convergence history with fitted (solid lines) and unfitted (dashed lines).

Unfitted Mesh - Convergence

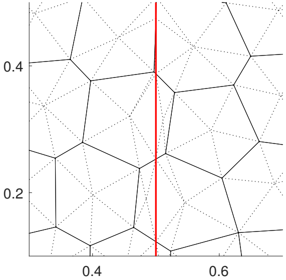

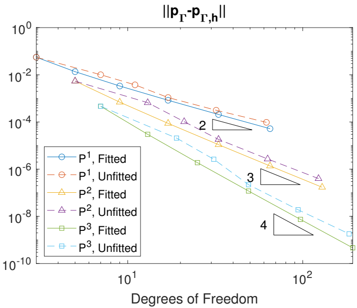

Figure: Convergence history with fitted (solid lines) and unfitted (dashed lines).

Numerical Experiments - Curved Fracture

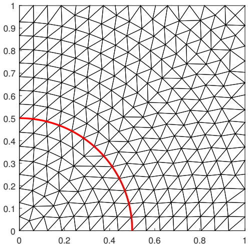

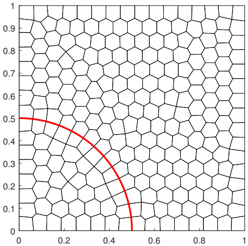

Figure: Fitted mesh using triangles (left) and polygons (right)

Numerical Experiments - Curved Fracture

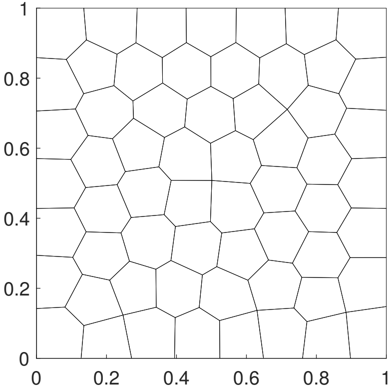

Figure: Cut mesh from a background mesh

Numerical Experiments - Curved Fracture

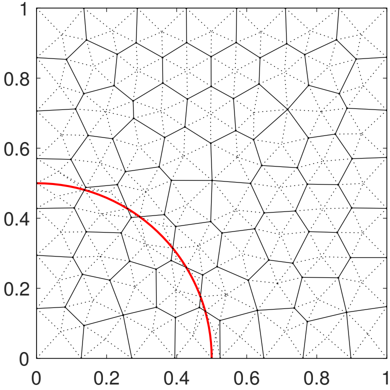

Figure: Cut mesh from a background mesh

Numerical Experiments - Curved Fracture

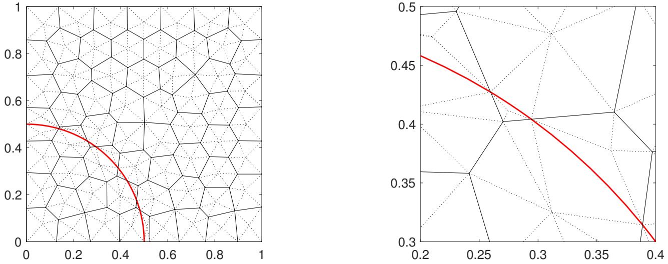

Figure: Cut mesh and its magnified view

Numerical Experiments - Curved Fracture

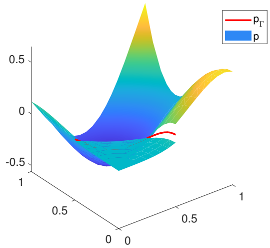

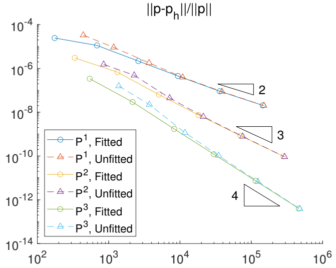

Figure: Solution shape (left) and convergence history with respect to degrees of freedom (right)

Quarter-Five Spot

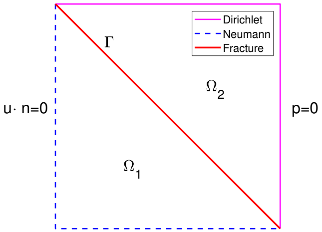

Figure: Domain configuration.

We set the boundary condition

$$\boldsymbol{u} \cdot \boldsymbol{n} = 0 \text{ on } \partial\Omega_1 \backslash \Gamma, \quad p = 0 \text{ on } \partial\Omega_2 \backslash \Gamma.$$

We model the injection and production by the source term

$$f = 10.1\Big(\tanh\Big(200(0.2 - (x^2 + y^2)^{\frac{1}{2}})\Big) - \tanh\Big(200(0.2 - ((x-1)^2 + (y-1)^2)^{\frac{1}{2}})\Big)\Big).$$

Quarter-Five Spot

We set

$$K = \begin{pmatrix} 1 & 0 \\ 0 & 1 \end{pmatrix}$$

and for (1) permeable fracture:

$$\kappa_\Gamma^n = 1, \quad \kappa_\Gamma^* = 100$$

and for (2) impermeable fracture:

$$\kappa_\Gamma^n = 0.01, \quad \kappa_\Gamma^* = 1.$$

Background mesh: Uniform rectangular mesh with $h_e = 2^{-6}$.
Cubic polynomials are used.

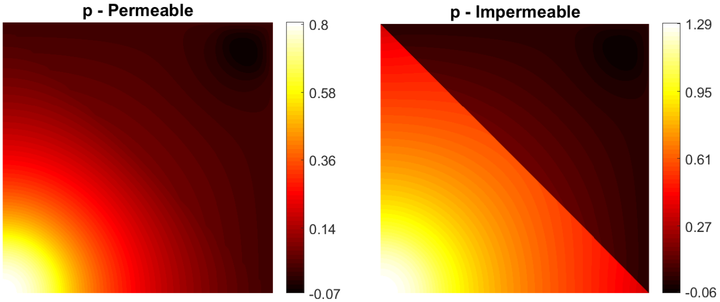

Figure: Pressure profile for the quarter-five spot problem with permeable (left) and impermeable (right) fracture.

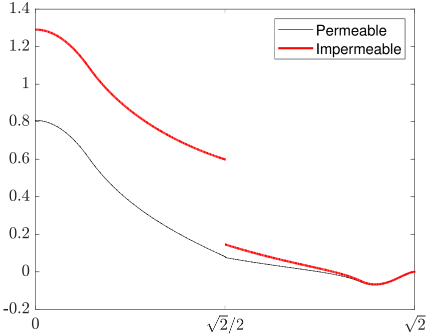

Figure: Pressure profile along $x = y$ for the quarter-five spot problem.

Outline

Conclusion and outlook

- Lowest order SDG methods on general meshes (FVM) for Poisson/Stokes/Elasticity problem
- Reliable (and efficient) a posteriori error estimations for Poisson/Stokes equations
- Locking free error estimates for the elasticity problems
- Generalization to high order polynomial approximations (Darcy-Forchheimer and Stokes coupled problem)
- Darcy flows in fractured porous media
- Interface problems and unfitted meshes, small/curved edges

References

• L Zhao and E-J Park, A staggered DG method of minimal dimension on quadrilateral and polygonal meshes, SIAM J. Sci. Computing 40(4) 2018, A2543-A2567.

• L Zhao, E-J Park, D Shin, A staggered DG method of minimal dimension for the Stokes equations on general meshes, Comput. Methods Appl. Mech. Engrg. 345 (2019), 854-875.

• L Zhao and E-J Park, A staggered cell-centered DG method for linear elasticity on polygonal meshes, SIAM J. Sci. Comput. 42 (2020), no. 4, A2158-A2181.

• L Zhao and E-J Park, A new hybrid staggered discontinuous Galerkin method on general meshes, Journal of Scientific Computing (2020).

• Dohyun Kim, L Zhao and E-J Park, Staggered DG Methods for the Pseudostress-Velocity Formulation of the Stokes Equations on General Meshes. SIAM J. Sci. Comput. 42 (2020), no. 4, A2537-A2560.

• L Zhao, E. Chung, E-J Park, and G. Zhou, Staggered DG method for coupling of the Stokes and Darcy-Forchheimer problems, SIAM J. Numer. Anal. 59 (1), 1–31, (2021).

• L Zhao, Dohyun Kim, E-J Park, E. Chung, Staggered DG Method with Small Edges for Darcy Flows in Fractured Porous Media, Journal of Scientific Computing (2022).

Thank You!

ICOSAHOM 2023

August 14-18, 2023

Yonsei University, Seoul, Korea

cf. ICIAM 2023, Tokyo, August 20-25, 2023